How important are diapycnal mixing and geothermal heating for the deep circulation of the Western Mediterranean?

Bruno Ferron, Pascale Bouruet-Aubertot, Yannis Cuypers, Katrin Schroeder, Mireno Borghini

AGU PUBLICATIONS

Geophysical Research Letters

RESEARCH LETTER
10.1002/2017GL074169

Key Points:
- Large observed dissipation rate of turbulent kinetic energy in Sicily Channel, Corsica Channel, and Ligurian Sea, weak elsewhere
- Geothermal heating brings threefold more buoyancy than small-scale turbulence to mix deep water masses below 1300 m
- Small-scale turbulence and geothermal heating do not bring enough buoyancy to balance upward advection of dense waters induced by western Mediterranean winter convection

Supporting Information:
- Supporting Information S1

Correspondence to:
B. Ferron,
bruno.ferron@ifremer.fr

Citation:
Ferron, B., P. Bouruet Aubertot, Y. Cuypers, K. Schroeder, and M. Borghini (2017), How important are diapycnal mixing and geothermal heating for the deep circulation of the Western Mediterranean?, *Geophys. Res. Lett.*, *44*, 7845–7854, doi:10.1002/2017GL074169.

Received 15 MAY 2017
Accepted 2 JUL 2017
Accepted article online 7 JUL 2017
Published online 5 AUG 2017

How important are diapycnal mixing and geothermal heating for the deep circulation of the Western Mediterranean?

B. Ferron[1], P. Bouruet Aubertot[2], Y. Cuypers[2], K. Schroeder[3], and M. Borghini[4]

[1]University of Brest, CNRS, IFREMER, IRD, Laboratoire d'Océanographie Physique et Spatiale, IUEM, Brest, France, [2]LOCEAN-IPSL, Sorbonne University (UPMC, University of Paris 06)-CNRS-IRD-MNHN, Paris, France, [3]CNR ISMAR—Arsenale, Venice, Italy, [4]CNR-ISMAR, Sede di La Spezia, Pozzuolo di Lerici, Italy

Abstract The dissipation rate of turbulent kinetic energy ε and the associated diapycnal turbulent mixing is inferred from a set of microstructure observations collected over several cruises from year 2012 to 2014. The geographical distribution of ε highlights several regions of enhanced levels of turbulence ranging from 10^{-9} to 10^{-6} W kg^{-1}: the Sicily Channel, the Corsica Channel, and the Ligurian Sea. Elsewhere, ε was small, often below 10^{-10} W kg^{-1}. Below 1300 m, geothermal heating provides three-fold more buoyancy than small-scale turbulence. Geothermal heating and turbulent diffusion provide enough buoyancy to balance 15% to 50% of a mean yearly deep water formation rate of 0.9 to 0.3 sverdrup (10^6 m^3/s), respectively. The remaining part has to eventually overflow through the Strait of Gibraltar.

Plain Language Summary During the winter season in the western Mediterranean, an invisible river transports dense waters formed at the surface by cold winds down to the ocean bottom at a rate sixfold larger than the Amazon River discharge. This winter flow increases the volume of dense waters present at depth. However, two mechanisms supply buoyancy and erode the volume of dense waters. One is heat coming from the seafloor and is called geothermal heating. The other is heat coming from the surface and is powered by natural fluid turbulence, in the same way as producing turbulence with a teaspoon mixes milk and tea vertically. Here we use historical data of geothermal heating and observations collected in 2012–2014 that measure for the first time the intensity of the oceanic turbulence to diagnose whether the winter volume increase of dense water at depth can be balanced by heat coming from the surface and the seafloor. Observations suggest that geothermal heating is threefold more efficient than oceanic turbulence in bringing heat to the dense waters at depth. But the addition of heat by both oceanic turbulence and geothermal heating is not strong enough to erode the import of winter dense water at depth.

1. Introduction

The western Mediterranean Sea is known to be an area of deep water (DW) formation since the pioneering observations by *Nielsen* [1912] and *Tchernia* [1956]. Using 600 hydrological stations, *Wüst* [1961] proposed the first synthesis of the Mediterranean thermohaline circulation, highlighting regions of water mass transformation due to air-sea interactions. The Gulf of Lion and the Ligurian Sea are open sea regions where the surface Atlantic Water is transformed into DW after mixing with the relatively warm and salty Levantine Intermediate Water (LIW) [*MEDOC Group*, 1970; *Sparnocchia et al.*, 1995]. Shelf waters surrounding the Gulf of Lion may get dense enough to cascade along the continental slope, thus contributing to the DW production [*Bougis and Ruivo*, 1954; *Bethoux et al.*, 2002; *Canals et al.*, 2006; *Durrieu de Madron et al.*, 2013].

The amount and properties of DW formed each winter present a large interannual variability mostly driven by the variability in the surface buoyancy loss and in the autumn stratification (both explain 70% of the DW formation variance [*Somot et al.*, 2016]). Several rates of DW formation were estimated using climatological observations and forcings, in situ observations, and modeling studies (Table S1 and section S2 in the supporting information with additional references [*Lascaratos*, 1993; *Tziperman and Speer*, 1994; *Rhein*, 1995; *Ulses et al.*, 2008; *Houpert et al.*, 2016]). Extreme events of DW formation significantly changed DW properties [*López-Jurado et al.*, 2005; *Schroeder et al.*, 2006; *Schroeder et al.*, 2008; *Smith et al.*, 2008]. Intense yearly DW formation rates of 2.4 sverdrup (10^6 m^3/s) (Sv) and 1.8–2.8 Sv were estimated for the 2004–2006 period [*Schroeder et al.*, 2008] and the 2012–2013 winter [*Waldman et al.*, 2016], respectively. Using a modeling study over the 1980–2013 period, *Somot et al.* [2016] showed that the yearly DW formation rate was larger than 0.6 Sv for 5 years, within 0.05–0.6 Sv for 14 years, and

smaller than 0.05 Sv for 14 years. The injection of dense water at depth by cascading along continental slopes was observed episodically [*Bethoux et al*., 2002]. Recent intense winter episodes of dense shelf water cascading occurred during 1999, 2005, 2006, and 2012 [*Font et al*., 2007; *Puig et al*., 2013; *Durrieu de Madron et al*., 2013]. About 0.03–0.07 Sv of DW was formed each of those years (Table S1). Using the published estimates, a long-term average of the yearly DW formation rates ranging from 0.3 to 0.9 Sv was found (section S2 in the supporting information).

Once injected at depth, the newly formed DWs are advected away from the convection region by boundary currents [*Send et al*., 1995], eddies, and submesoscale coherent vortices (SCVs) [*Testor and Gascard*, 2003, 2006] and invade the various subbasins of the western Mediterranean Sea [*Millot and Taupier-Letage*, 2005]. Whatever the spreading dynamics, any advection of newly formed DWs increases the volume of the DWs of the same density class in the western basin, which tends to uplift lighter water masses [*Font et al*., 2009; *Bryden*, 2009; *Rohling et al*., 2015]. Such an uplift is usually not easily captured by observations because of the weak property contrasts at depth between newly formed and older ambient dense waters. However, during the strong convection events of 2004–2006 and 2009, the uplifting of older resident DWs by several hundreds of meters was clearly evidenced on short time scales of a few years [*Schroeder et al*., 2008, 2016; *Fuda et al*., 2009]. On longer time scales, the uplifting trend can be balanced by (1) a direct outflow of dense waters through the Strait of Gibraltar and (2) an erosion of DW properties induced by buoyancy inputs from shallower depths by diapycnal turbulent mixing and from the seafloor by geothermal heating. If the balance was done with the outflow, no significant diapycnal mixing would be required and the dense circulation would be mostly adiabatic. Applying Bernoulli's conservation law along streamlines, *Stommel et al*. [1973] estimated that waters as deep as 1300 m can be drawn over Gibraltar sill and flow out in the Atlantic. This makes assumption (1) plausible. If the balance is reached via buoyancy input, the dense circulation would be strongly diabatic.

Among the two diabatic processes listed above (geothermal heating and diapycnal mixing), the intensity and distribution of the diapycnal mixing due to small-scale turbulence has the largest uncertainty. Indeed, no direct microstructure measurement exists at depth to quantify the intensity of turbulent processes in the Mediterranean. Oceanic microstructure was sampled over the shallow Cyclades Plateau to a maximum depth of 500 m [*Gregg et al*., 2012] and in the upper 100 m along a zonal Mediterranean transect [*Cuypers et al*., 2012]. In the latter study, a fine-scale parameterization was used to indirectly estimate the vertical eddy diffusivity from the surface to the bottom.

The setting of the deep stratification, the impact of the turbulent mixing, and the geothermal heating on the deep thermohaline circulation in the western Mediterranean are the focus of this study. We estimate the role of the diapycnal mixing via a unique set of full depth microstructure profiles that were mostly sampled in 2013 and 2014. In addition, the importance of the geothermal component on the modification of DW masses is quantified using available estimates.

2. Materials and Methods

2.1. Microstructure Data Set

Our microstructure data set is composed of seven cruises made between April 2012 and December 2014 (Table S2). Two of them, made on board the R/V *Europe* remained on the continental slope off Toulon. The remaining cruises, on board the R/V *Urania*, visited various subbasins of the western Mediterranean Sea to monitor the spatial and temporal ocean variability.

The data set comprises 148 full depth microstructure profiles distributed over 71 stations and sampled with two vertical microstructure profilers VMP-6000. Nearly 51% of the stations were sampled more than once, sometimes during the same cruise or, more frequently, during different cruises (Figure 1a). Most of the profiles were located in the Tyrrhenian Sea, the Algerian Basin, the Sardino-Balearic Abyssal Plain, and the Ligurian Sea. The largest number of repeated profiles was sampled in the Sicily Channel (also named Sicily Strait) and in the Corsica Channel. A few profiles were made in the Ionian Sea, off Catania.

Dissipation rates of turbulent kinetic energy were estimated from the variance in the vertical shear of horizontal velocities measured at centimetric scale by two shear probes mounted on each VMP. Assuming isotropy,

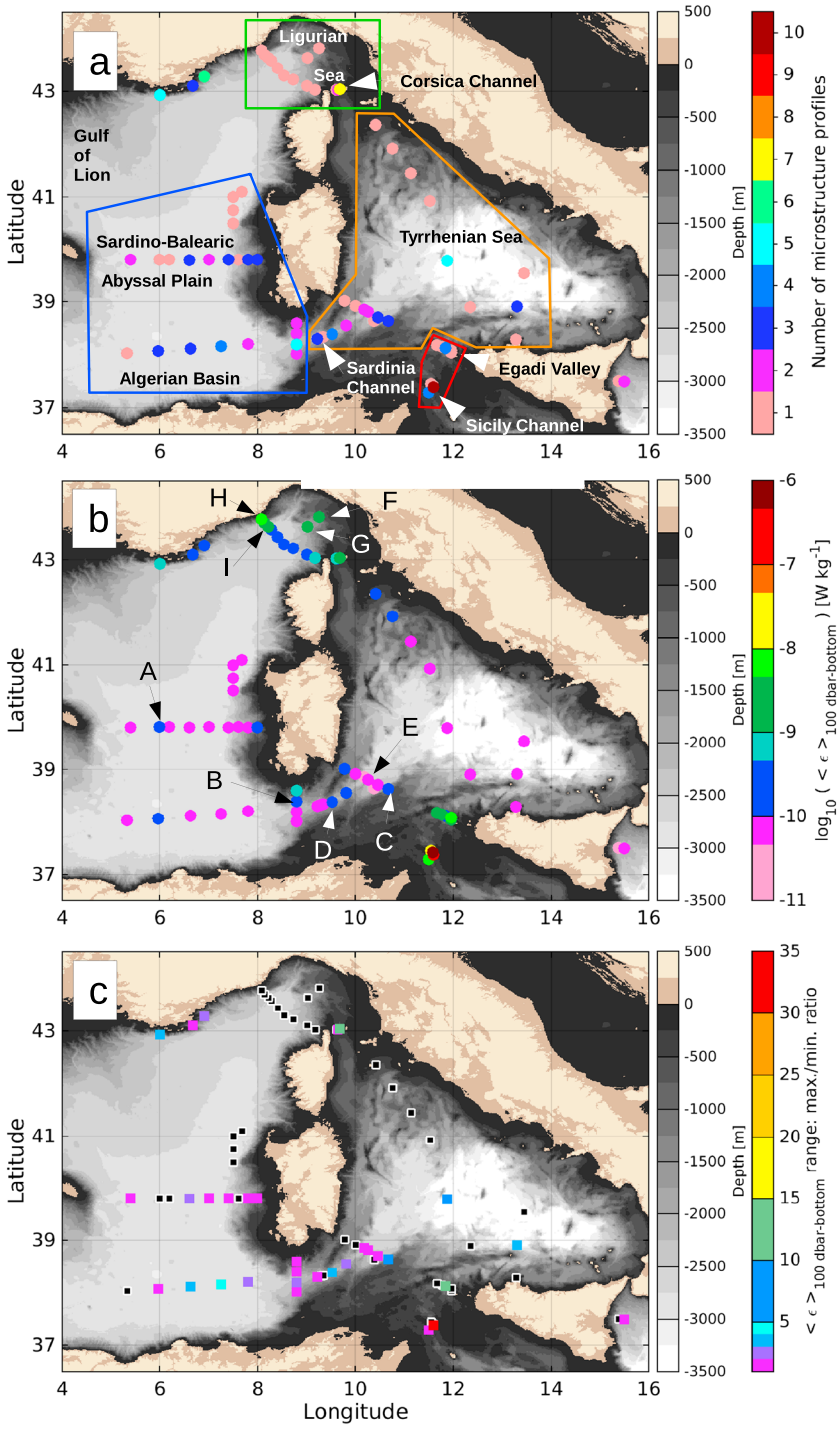

Figure 1. (a) Location of microstructure stations, number of vertical profiles available at each station, and regional boxes used in Figure S1. (b) Depth-averaged dissipation rate below 100 m (log scale, W kg^{-1}); letters denote locations of enhanced dissipation profiles below 1000 m (Figure S1). (c) Maximum to minimum ratio of the depth-averaged dissipation rate for stations having at least two profiles (note the nonlinear color scale; stations with a unique profile are represented with a black square surrounded by white). Bathymetry from *Smith and Sandwell* [1997, v. 18.1].

the dissipation rate of turbulent kinetic energy per unit mass reads $\varepsilon = 7.5\ \nu \langle u_z^2 \rangle$, where ν is the viscosity of seawater and $\langle u_z^2 \rangle$ is the variance in the vertical shear of the horizontal velocity. For further details on the microstructure data processing, the reader is referred to *Ferron et al.* [2014, section 2a]. Microstructure profiles were usually stopped 90 m above the seafloor.

2.2. Geothermal Heating

Several studies have estimated the geothermal heat flux from the lithosphere to the ocean west of Corsica and Sardinia and in the Tyrrhenian Sea. In the Gulf of Lion, *Burrus et al*. [1987] estimated that the heat flux was in the range of 50 to 70 mW m^{-2}. *Pasquale et al*. [1996a] estimated a mean geothermal flux for the Ligurian-Provençal Basin of 105 ± 20 mW m^{-2}. For the Algerian and Alboran Basins, the mean heat flux estimate was 107 ± 18 mW m^{-2} [*Pasquale et al*., 1996b]. For our study, we used an average value of 100 mW m^{-2} for all subbasins located to the west of Corsica and Sardinia Islands. In the Tyrrhenian Sea south of 41°N, the mean geothermal heat flux was larger and reached about 135 mW m^{-2}, for depths larger than 1000 m, peaking up to 157 mW m^{-2} in the central Magnaghi-Vavilov Basin and to 171 mW m^{-2} in the eastern Marsili Basin [*Pasquale et al*., 1999]. In the deep Tyrrhenian Sea north of 41°N, *Mongelli et al*. [2004] reported values that were centered around 120 mW m^{-2}. Thus, we used a mean value of 130 mW m^{-2} for the whole Tyrrhenian Sea.

2.3. Diapycnal Velocity and Small-Scale Turbulence

The diapycnal velocity w_d^K associated with the vertical turbulent diffusion K due to small-scale turbulence was diagnosed using the balance between advective buoyancy fluxes and the vertical divergence of turbulent diffusive fluxes of buoyancy (see supporting information, method with additional references [*McDougall*, 1991; *McDougall and You*, 1991]):

$$w_d^K \frac{1}{\rho_\theta} \partial_z \rho_\theta = \partial_z \left(K \frac{1}{\rho_\theta} \partial_z \rho_\theta \right) \tag{1}$$

Due to the presence of a homogeneous bottom boundary layer and to a no flux of heat and salt between seawater and the ground, a no-buoyancy flux condition is used at the seafloor [*de Lavergne et al*., 2016]. This boundary condition implies that turbulent motions create a convergence of buoyancy near the seafloor that must be compensated by an upward advection according to equation (1).

In the following, the vertical eddy diffusivity denoted as K_B will refer to *Bouffard and Boegman*'s [2013] parameterization with the four mixing regimes (see supporting information, method with the additional reference [*Shih et al*., 2005]). The vertical eddy diffusivity K_O from the Osborn parameterization that uses a constant mixing efficiency Γ of 0.2 will be calculated in some cases to illustrate the difference with K_B, since K_O has been widely used in the literature so far regardless of the existence of the mixing regimes.

In order to diagnose the diapycnal velocity from direct ε measurements, western Mediterranean averaged quantities were formed by first calculating a station-averaged profile as a function of potential density referenced at 2000 dbar before averaging over all the stations. Data from the Ionian Sea and the Sicily Channel were excluded from the basin average since they do not erode DWs formed in the western basin.

2.4. Bathymetric Roughness

The 1 min gridded Global Topography version 18.1 [*Smith and Sandwell*, 1997], which resolves scales larger than 10–20 km, was used to compute topographic roughness. Following *Morris et al*. [2001], the roughness was computed as the root-mean-square of topographic perturbations present in a 6 min × 6 min square. Topographic perturbations were defined as the difference between the Global Topography and the 2-D Gaussian filtered version of the Global Topography. The Gaussian filter had a 10 min × 10 min size with a standard deviation of 2min.

3. Results

The dissipation rate averaged below a depth of 100 m, $<\varepsilon>$, ranged from 4×10^{-11} to 7×10^{-6} W kg^{-1}. The smallest values were found in the Ionian Sea and to the southwest of the Tyrrhenian Sea, while the largest value was found in the Sicily Channel (Figure 1b). In the Tyrrhenian Sea, the Algerian Sea, and the Sardino-Balearic Abyssal Plain, $<\varepsilon>$ was quite weak ($< 1 \times 10^{-10}$ W kg^{-1}) or moderately weak ($1–5 \times 10^{-10}$ W kg^{-1}). Slightly moderate $<\varepsilon>$ ($1–5 \times 10^{-9}$ W kg^{-1}) was found in the Corsica Channel, associated with the northward flow of Atlantic Water (AW) and LIW, and in the downstream cyclonic boundary current in the Ligurian Sea. Slightly moderate $<\varepsilon>$ was also found above the Egadi Valley (northwest of Sicily) possibly in relation with the inflow of AW into the Tyrrhenian Sea in the upper

water column and of LIW and transitional Eastern Mediterranean Deep Water (tEMDW) in the lower water column [e.g., *Onken et al.*, 2003].

For stations that have repeated profiles, the ratio between the maximum and the minimum $<\varepsilon>$ showed a weak temporal variability over the cruises (Figure 1c). Indeed, 60% of the ratios were below a factor of 3 for a quantity that can vary over several orders of magnitude. The ratio was larger than 10 only at three stations located in the Corsica Channel, the Sicily Channel, and the Egadi Valley. This shows the strong contrast between stations where the dynamics is relatively stable, leading to a relatively small variability in $<\varepsilon>$ over time, and those with systematic temporal variability as a result of active turbulent processes. There, the onset of small-scale instabilities is strongly related to the fluid dynamics that varies seasonally and interannually (changes in the surface forcing, in the internal wavefield, and in shears of horizontal currents).

In the Sardino-Algerian Sea (Figure 1a, blue box), dissipation rates below 1000 m are almost systematically smaller than 10^{-10} W kg^{-1} at the exception of two profiles which exhibit a bottom enhanced turbulence (profiles A and B, Figures 1b and S1a). Profile A is located off the Balearic Islands at 5°59.16′E, 39°48.11′N (2800 m depth) and profile B lies on the northern slope of the Sardinia Channel (1300 m depth). The former is unique in our data set and shows vertical properties of temperature, salinity, and density very similar to the anticyclonic SCV of Western Mediterranean Deep Water (WMDW) observed by *Bosse et al.* [2016, Figure 4a]. At a given depth, the scatter in the ε profiles was estimated as the RMS of the ratio between the profiles and their average (Figure S1a, solid thick and dashed colored profiles). For the Sardino-Algerian Sea, the RMS ratio below 1000 m is weakly dependent on depth and reaches 1.6 (increases to 2.9 at the bottom due to profile A). In the Tyrrhenian Sea, the scatter in the dissipation profiles is similar and reaches 1.7 on average below 1000 m (Figure S1b). A few profiles, all located near ridges, seamounts, or continental slopes, exhibit some peaks in ε off the bottom (profiles C to E, Figures 1b and S1b). Profile C, located on the southern slope of the Cornaglia Basin, is the most noticeable with a fivefold increase in ε compared to the mean profile between 1000 and 1400 m. In the Ligurian Sea, profiles from F to I (Figures 1b and S1c), all located along the continental slope where the Liguro-Provençal current flows, show dissipation rates that are an order of magnitude larger than those off the slope over most of the water column. In the Sicily-Egadi region, a large scatter of 13 is found in ε due to the presence of the turbulent overflow in the Sicily Channel that coexists with the more quiescent downstream flow in the Egadi Valley (Figures 1b and S1d).

In the DWs of the Sardino-Balearic Sea and Algerian Sea, the eddy diffusivity K_B is weak as it ranges from 0.1 to 1×10^{-4} m^2 s^{-1} (Figure 2a). In the Tyrrhenian Sea, K_B is slightly larger and shows several peaks above 1×10^{-4} m^2 s^{-1} that are due to the presence of very weakly stratified waters and not to an enhanced level of turbulence (Figures 2b and S1b). In the Ligurian Sea, K_B lies in the range $1–3 \times 10^{-4}$ m^2 s^{-1} from the level of the LIW to the deepest water mass (Figure 2c). By contrast with the Tyrrhenian Sea, those moderate eddy diffusivity values are sustained by an increase in the level of turbulence as highlighted by the ε profiles located along the continental slope and their depth-averaged values (Figures S1c and 1b). In the Sicily Channel, K_B is the largest and exceeds 30×10^{-4} m^2 s^{-1} (Figure 2d). From the depth of the LIW down to the tEMDW, K_B rarely drops below 1×10^{-4} m^2 s^{-1} as it is sustained by a strong level of turbulence (Figures 1b and S1d). Further downstream in the Egadi Valley, K_B falls back to the weak values observed in the deep basins ($K_B < 1 \times 10^{-4}$ m^2 s^{-1}) with the exception of one K_B-enhanced station, associated with the dense overflow from the Sicily Channel that exhibits values larger than 1×10^{-4} m^2 s^{-1} and a mixing line pointing toward the θ-S properties of the tEMDW found at the Sicily Channel (Figure 2d).

The western basin-averaged profile of ε varies within a factor of 2 between $\sigma_2 = 37.6$ kg m^{-3} (averaged depth of 230 m) and $\sigma_2 = 37.757$ kg m^{-3} (1800 m) before dropping by a factor of 16 down to the densest water masses found in the Ligurian and Sardino-Algerian Seas (Figure 3a, black line; see Figure 3b, magenta line, to get the basin-averaged depth of a σ_2 density anomaly). No sign of decrease in ε is found as a function of height above the bottom (Figure 3a, inset) despite the occurrence of few deep bottom-enhanced turbulence (Figure S1). This can be due to an undersampling of the regions with rough bathymetry that frequently leads to bottom-enhanced turbulence [e.g., *Polzin et al.*, 1997; *Nash et al.*, 2004; *Ferron et al.*, 2016; *Pasquet et al.*, 2016] or to a lack of energy source at depth, such as internal tides. The basin-averaged eddy diffusivity K_B increases with density below $\sigma_2 = 37.6$ kg m^{-3} from 0.1×10^{-4} m^2 s^{-1} to values slightly larger than 1×10^{-4} m^2 s^{-1} at depth (Figure 3c, black line). This increase in K_B, observed in all subbasins, is due to the large decrease in buoyancy frequency with density (Figure 3a, magenta line). For comparison, the Osborn

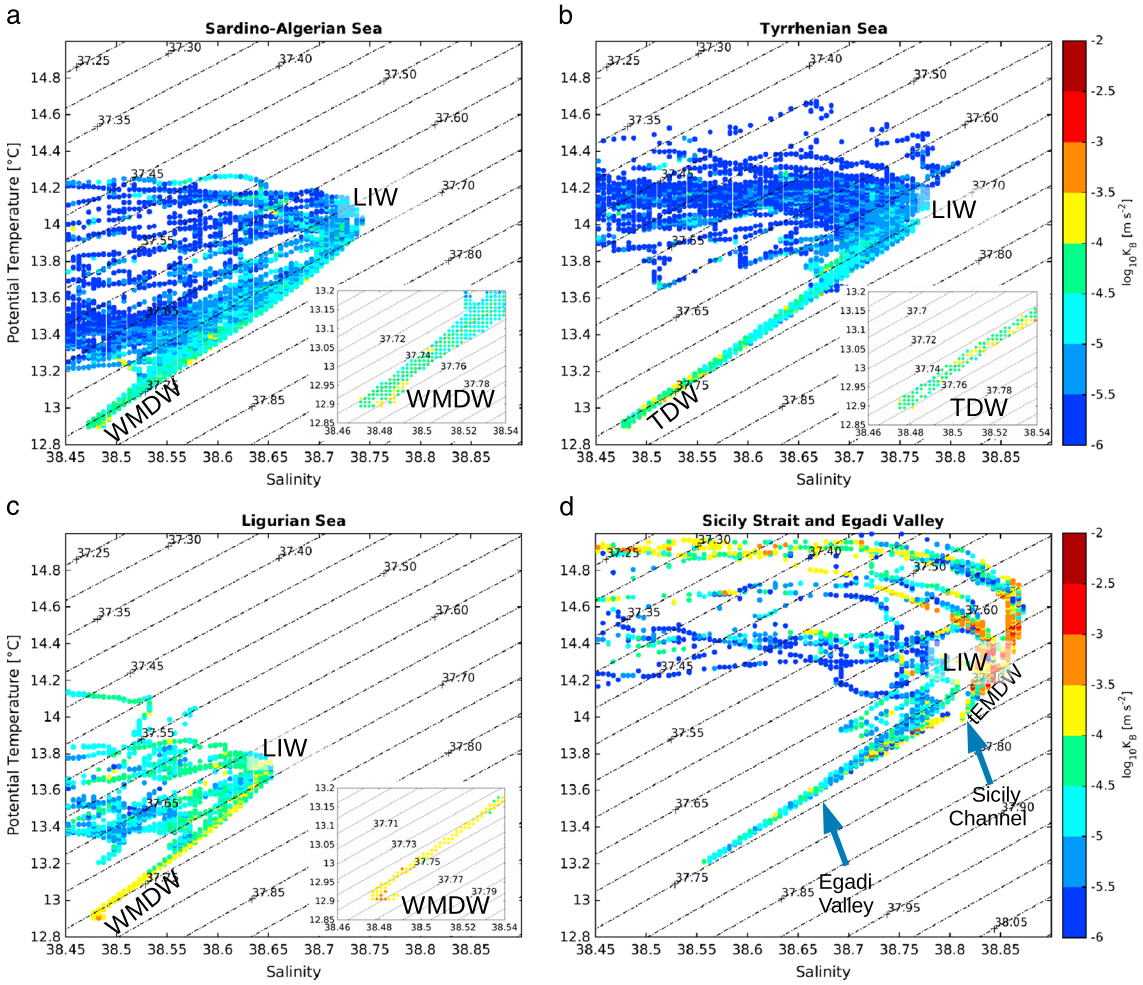

Figure 2. Regional potential temperature-salinity diagrams and magnitude of the eddy diffusivity K_B. WMDW: Western Mediterranean Deep Water, TDW: Tyrrhenian Deep Water, tEMDW: transitional Eastern Mediterranean Deep Water, LIW: Levantine Intermediate Water. Insets show an enlargement of the deep water regions.

diffusivity K_O exceeds the Bouffard diffusivity K_B by mean factor of 4 below σ_2 = 37.73 kg m^{-3} (averaged depth of 800 m; Figure 3c, solid and black dashed lines). The diffusive buoyancy flux using K_B decreases by a factor of 4 between σ_2 = 37.70 kg m^{-3} (500 m) and σ_2 = 37.76 kg m^{-3} (2400 m) and by another factor of 3 down to the largest density (Figure 3d). Given equation (1) and its no-flux boundary condition, the large-scale vertical gradient in the diffusive buoyancy flux is positive and therefore able to balance mean DW upward velocities of 7×10^{-8} m s^{-1} at an averaged depth of 1000 m and 1500 m, 4×10^{-8} m s^{-1} at 2000 m, and 20×10^{-8} m s^{-1} at 2600 m over the western basin. Accounting for the depth-dependent area of the basin, such vertical velocities correspond to a transport of 0.04 Sv at 1000 m and 1500 m, 0.02 Sv at 2000 m, and 0.1 Sv at and below 2600 m. The large-scale decrease in the diffusive buoyancy flux is observed in all subbasins, tough weaker in the Tyrrhenian Sea (factor of 2 from 37.70 kg m^{-3} to 37.76 kg m^{-3}) than in the Ligurian and Sardino-Algerian Seas (factors of 4 and 6, respectively). The largest DW upward velocities are found in the Ligurian Basin as they decrease from of 14×10^{-8} m s^{-1} to 8×10^{-8} m s^{-1} from 1000 to 1800 m and increase up to 30×10^{-8} m s^{-1} below. In the Sardino-Algerian Basin, the DW upward velocity decreases from 5×10^{-8} m s^{-1} to 2×10^{-8} m s^{-1} from 1000 to 2500 m and then increases to 60×10^{-8} m s^{-1} near the bottom. In the Tyrrhenian Sea, the upward velocity is the weakest and ranges from 0.2 to 0.6 $\times 10^{-8}$ m s^{-1} below 1000 m. In contrast with the Bouffard parameterization, the western basin diffusive buoyancy flux using the Osborn parameterization is more stable above σ_2 = 37.759 kg m^{-3} (2000 m; Figure 3d, solid and black dashed lines). The only large positive gradient able to balance an averaged DW upward advection of 0.3 Sv is found below 2000 m.

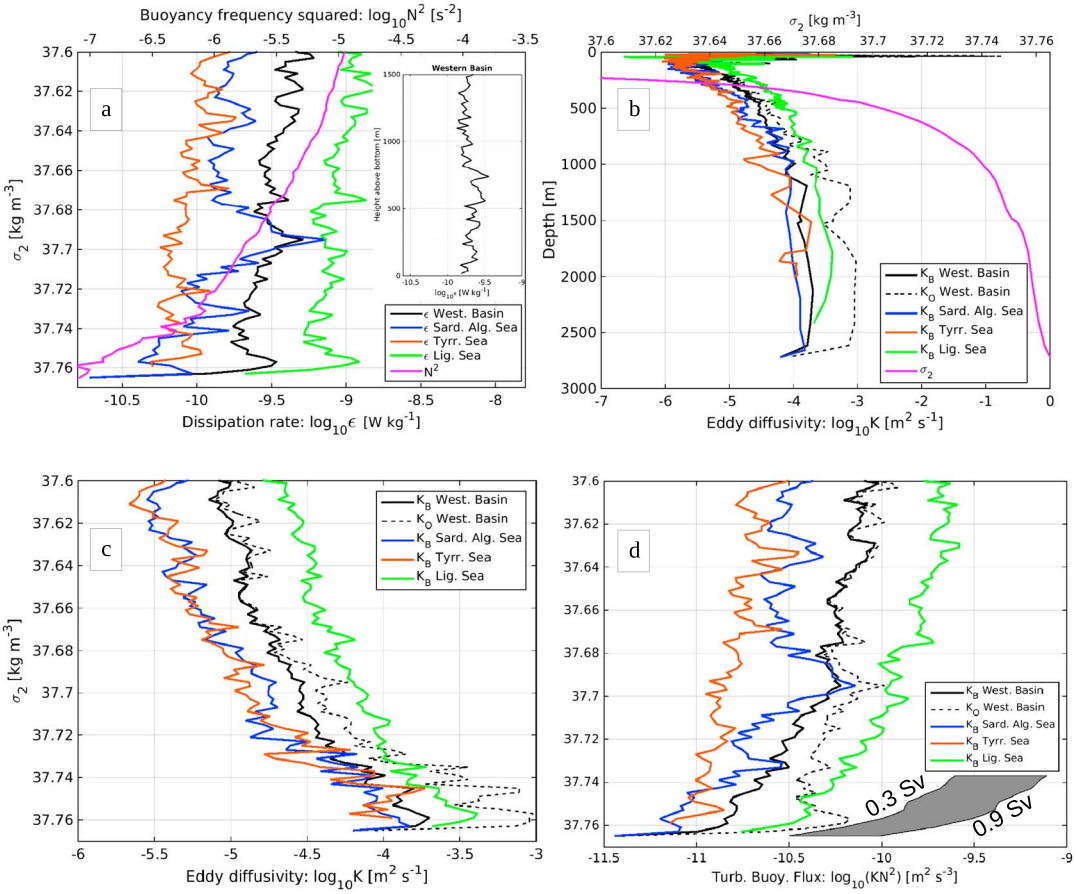

Figure 3. Western basin-averaged (black, magenta) and regional-averaged (other colors) profiles of (a) buoyancy frequency squared and dissipation rate versus potential density anomaly referenced to 2000 dbar, σ_2; inset: average of the western basin dissipation rate profiles deeper than 1500 m versus height above bottom. (b) Eddy diffusivity and σ_2 versus basin-averaged depth level of σ_2 isopycnals. (c) Turbulent diffusivity and (d) turbulent diffusive buoyancy flux according to Bouffard (K_B, solid) and Osborn (K_O, dashed) parameterizations. The gray-shaded region delimits the theoretical buoyancy flux needed to balance a yearly DW formation rate of 0.3–0.9 Sv as determined from equation (1). Station-mean profiles were first computed as a function of σ_2 before averaging the stations together.

4. Discussion and Conclusion

With a mean yearly DW formation rate ranging from 0.3 to more than 0.9 Sv as diagnosed from observations (Table S1 and section S2 in supporting information), it becomes obvious that the observed diffusive buoyancy flux gradient is 1–2 orders of magnitude too weak to balance the uplifting of annually formed DWs below 1000 m (Figure 3d, gray-shaded region).

What is the robustness of this dissipation rate data set at depth? Could we have missed important regions and/or periods that would strongly increase the diffusive buoyancy flux gradient in the deep sea? We "only" have about 150 full depth and instantaneous profiles in hand. However, those profiles cover several basins; they are located in various dynamical regions (open ocean, narrow passages, and along shelf edge) and were taken at different seasons. A small temporal variability over the cruises was observed for the deep stations (86% of repeated stations show an averaged dissipation rate below 1000 m that remains below a factor of 5). Furthermore, this study focuses on the upward advection of DWs for which turbulence sources are limited (as opposed to the upper ocean). The largest source of turbulence at depth is expected to be due to the breaking of internal wave and current-topography interactions [*Ferrari and Wunsch*, 2009]. Temporal variability in ε is expected from the downward propagation of wind generated near-inertial waves. In the Northwest Pacific at 35–40°N and at 400 m depth, *Whalen et al*. [2012] showed that ε was larger by a factor of 8 in winter than in summer due to winter storms. Using current-meter data in the Northeast Pacific at 50°N, *Alford et al*. [2012] showed that downward propagating near-inertial energy was indeed larger in winter than in summer

by a factor of 4 at 400 m but only by a factor of 2 at 800 m. Given that the Mediterranean Sea has much weaker wind power input to the ocean than the Northwest Pacific and given the decrease of near-inertial energy with depth, ε should not change from summer to winter by more than a factor of 2 below 1000 m. The presence of rough topography is also a major ingredient to enhance the level of turbulence as a few profiles highlighted in this study (Figure S1). In order to diagnose whether a sampling bias relative to the bathymetric roughness exists, we followed *Huussen et al.*'s [2012] approach and compared the probability density distribution of roughness at the microstructure stations and at the scale of the whole western Mediterranean Basin (Figure S2 in supporting information). The western Mediterranean Basin is relatively smooth, about 50% of the area having a roughness smaller than 50. This is especially true for the western-most subbasins. The most pronounced roughness is located along shelves, narrow passages, and in the Tyrrhenian Sea. The distribution of roughness at the microstructure stations only shows a very little bias toward larger roughness. Thus, the fact that the vertical gradient in the turbulent buoyancy flux is too weak to balance the DW upward advection cannot be attributed to a lack of microstructure profiles over rough topography. Spatial and temporal enhanced levels of turbulence at depth over flat topography can also be induced by SCVs having a depth-intensified component [*Testor and Gascard*, 2006]. *Bosse et al.* [2016] estimated that 52–83 depth-intensified SCVs were formed and coexisted throughout the year (not accounting for surface-intensified cyclonic SCVs). A unique VMP station sampled a SCV over the 71 stations as highlighted by profile A (Figure S1). Given a typical SCV radius of 5–8 km [*Bosse et al.*, 2016] and the area deeper than 2000 m (4×10^5 km^2), this unique station is equivalent to contribute a total of 28–72 depth-intensified SCVs in the western average profiles. The contribution of SCVs able to mix the deep waters seems reasonably taken into account given that the number of SCVs by *Bosse et al.* [2016] was inferred for winters 2010–2013, all characterized by strong bottom-reaching deep convection in the Gulf of Lions.

The contribution of the geothermal heating Q_G to the increase with time in buoyancy of western Mediterranean DWs can be estimated as $g\alpha Q_G/(\rho C_p h)$, with α (2.34°C^{-1}) the temperature expansion coefficient of the layer, C_p (3980 J kg^{-1} °C^{-1}) the heat capacity of seawater, and h (1200 m) the mean layer thickness of DWs below 1300 m. As outlined in section 2, Q_G is on average 30% larger in the Tyrrhenian Basin than to the west of Corsica and Sardinia. Taking the respective subbasin areas into account, the averaged geothermal heating amounts to a value close to 110 mW m^{-2} for the whole western Mediterranean. Thus, the geothermal heating induces an increase in buoyancy with time of 5.1×10^{-14} m s^{-3} for DWs below 1300 m. For comparison, the turbulent diffusion brings a buoyancy flux of 2×10^{-11} m^2 s^{-3} at depth of 1300 m (Figure 3d, solid black line at σ_2 = 37.745 kg m^{-3}), which gives a time increase in buoyancy close to 1.7×10^{-14} m s^{-3} for the 1200 m thick DWs. Hence, the buoyancy increase by the geothermal heating is threefold that produced turbulent diffusion.

The error in the basin-averaged geothermal heating may be as large as 30% considering uncertainties in measurements, sampling biases, and averaging errors, which gives a 30% error in the increase with time in buoyancy. The error associated with the turbulent diffusion is more difficult to assess. Indeed, it not only involves errors in obtaining a good representation of the basin-scale ε but it also involves error in the parameterization of the turbulent diffusion itself. For the former error, a relative robustness was found regarding temporal variability and the representativity of enhanced profiles due to topographic roughness and SCVs, thus suggesting a contained error, probably smaller than a factor of 3 in the basin-averaged buoyancy flux. The parameterization of the turbulent diffusion is still a field of active research. We used one of the most recent parameterizations supported by direct numerical experiments and ocean observations. The Bouffard parameterization makes a difference with the Osborn parameterization, but none of them produces a gradient in turbulent buoyancy fluxes able to balance the upward advection of DW masses above 2000 m.

Taken together, the geothermal heating and the turbulent diffusion can balance an upward transport of 0.1–0.15 Sv (resp. 0.2–0.25 Sv if the turbulent buoyancy flux gradient was underestimated by a factor of 3 and the geothermal heat flux by 30%). Thus, assuming that this data set gives a robust image of the turbulent mixing intensity as previously discussed, the geothermal heating and the turbulent diffusion could balance 15% to 50% (resp. 25–75%) of a mean yearly DW production rate of 0.9 to 0.3 Sv, respectively. The remaining 50–85% (resp. 25–75%) of the DW production rate has to eventually overflow through the Strait of Gibraltar [*García-Lafuente et al.*, 2007, 2009; *Millot*, 2009] supported by Bernoulli aspiration [*Stommel et al.*, 1973; *Rohling et al.*, 2015]. If mixing has a limited impact for the fate of DW masses at the scale of the whole

western Mediterranean Sea, it, however, certainly contributes to erode the properties of intermediate and deep waters in specific regions with elevated levels of turbulence such as the Sicily Channel, the Corsica Channel, the Ligurian Sea, and other unexplored locations.

Acknowledgments
We thank all crew members of R/V *Urania* and R/V *Europe* and Alberto Ribotti (CNR IAMC Oristano) for his contribution to the organization of the ICHNUSSA cruises. We thank anonymous reviewers who *helped to improve and clarify* this manuscript. The microstructure profilers were funded by the French Agence Nationale de la Recherche (ANR) through grant ANR-JC05_50690 and by the French Institute for Marine Science (IFREMER). This project was funded by CNR-ISMAR, LOCEAN, LOPS and the INSU-MISTRALS (Mediterranean Integrated STudies at Regional and Local Scales) program. B. Ferron was supported by the French National Center for Scientific Research (CNRS). This study contributes to the HyMeX program (HYdrological cycle in The Mediterranean Experiment). Data requests may be sent to the corresponding author.

References

Alford, M., F. Cronin, and J. M. Klymak (2012), Annual cycle and depth penetration of wind-generated near-inertial internal waves at Ocean Station Papa in the northeast Pacific, *J. Phys. Oceanogr.*, *42*, 889–909, doi:10.1175/JPO-D-11-092.1.

Bethoux, J. P., X. Durieu de Madron, F. Nyffeler, and D. Tailliez (2002), Deep water in the western Mediterranean: Peculiar 1999 and 2000 characteristics, shelf formation hypothesis, variability since 1970 and geochemical inferences, *J. Mar. Syst.*, *33–34*, 117–131.

Bosse, A., et al. (2016), Scales and dynamics of Submesoscale Coherent Vortices formed by deep convection in the northwestern Mediterranean Sea, *J. Geophys. Res. Oceans*, *121*, 7716–7742, doi:10.1002/2016JC012144.

Bougis, P., and M. Ruivo (1954), Sur une descente des eaux superficielles en profondeur (cascading) dans le sud du Golfe du Lion, *Bull. Inf. Comité Cent. Océanogr. Etude Côtes*, *6*, 147–154.

Bouffard, D., and L. Boegman (2013), A diapycnal diffusivity model for stratified environmental flows, *Dyn. Atmos. Oceans*, *61–62*, 14–34, doi:10.1016/j.dynatmoce.2013.02.002.

Bryden, H. L. (2009), Where does the new Mediterranean deep water go?, in *CIESM, 2009. Dynamics of Mediterranean Deep Waters*, *CIESM Workshop Monogr.*, vol. 38, edited by F. Briand, pp. 67-70, Monaco.

Burrus, J., F. Bessis, and B. Doligez (1987), Heat flow, subsidence and crustal structure of the Gulf of Lions (NW Mediterranean): A quantitative discussion of the classic passive margin model, in *Sedimentary Basins and Basin-Forming Mechanisms*, edited by C. Beaumont, and A. J. Tankard, *Mem.-Can. Soc. Pet. Geol.*, 12, 1-15.

Canals, M., P. Puig, X. Durrieu de Madron, S. Heussner, A. Palanques, and J. Fabres (2006), Flushing submarine canyons, *Nature*, *444*, 354–357.

Cuypers, Y., P. Bouruet-Aubertot, C. Marec, and J.-L. Fuda (2012), Characterization of turbulence from a fine-scale parameterization and microstructure measurements in the Mediterranean Sea during the BOUM experiment, *Biogeosciences*, *9*, 3131-3149.

de Lavergne, C., G. Madec, J. Le Sommer, A. J. G. Nurser, and A. C. Naveira Garabato (2016), The impact of a variable mixing efficiency on the abyssal overturning, *J. Phys. Oceanogr.*, *46*(2), 663–681.

Durrieu de Madron, X., et al. (2013), Interaction of dense shelf water cascading and open-sea convection in the northwestern Mediterranean during winter 2012, *Geophys. Res. Lett.*, *40*, 1379–1385, doi:10.1002/grl.50331.

Ferron, B., F. Kokoszka, H. Mercier, and P. Lherminier (2014), Dissipation rate estimates from microstructure and finescale internal wave observations along the A25 Greenland–Portugal OVIDE line, *J. Atmos. Ocean. Technol.*, *31*, 2530–2543, doi:10.1175/JTECH-D-14-00036.1.

Ferron, B., F. Kokoszka, H. Mercier, and P. Lherminier (2016), Variability of the diapycnal mixing along the A25 Greenland-Portugal transect repeated from 2002 to 2012, *J. Phys. Oceanogr.*, *46*, 1989-2003, doi:10.1175/JPO-D-15-0186.1.

Ferrari, R., and C. Wunsch (2009), Energy: Reservoirs, sources, and sinks, *Annu. Rev. Fluid Mech.*, *41*, 253–82, doi:10.1146/annurev.fluid.40.111406.102139.

Font, J., P. Puig, J. Salat, A. Palanques, and M. Emelianov (2007), Sequence of hydrographic changes in NW Mediterranean deep water due to the exceptional winter of 2005, *Sci. Mar.*, *71*(2), 339–346.

Font J., et al. (2009), *Dynamics of Mediterranean Deep Waters, CIESM*, *CIESM Workshop Monogr.*, vol. 38, edited by F. Briand, pp. 5-17, Monaco.

Fuda, J. L., et al. (2009), Recent dense water formation in the Mediterranean western basin, as observed by HYDROCHANGES, in *CIESM, 2009. Dynamics of Mediterranean Deep Waters*, *CIESM Workshop Monogr.*, vol. 38, edited by F. Briand, pp. 91-100, Monaco.

García-Lafuente, J., A. Sánchez Román, G. Díaz del Río, G. Sannino, and J. C. Sánchez Garrido (2007), Recent observations of seasonal variability of the Mediterranean outflow in the Strait of Gibraltar, *J. Geophys. Res.*, *112*, C10005, doi:10.1029/2006JC003992.

García-Lafuente, J., J. Delgado, A. Sánchez Román, J. Soto, L. Carracedo, and G. Díaz del Río (2009), Interannual variability of the Mediterranean outflow observed in Espartel sill, western Strait of Gibraltar. *J. Geophys. Res.*, *114*, C10018, doi:10.1029/2009JC005496.

Gregg, M., Alford M., Kontoyiannis H., Zervakis V., and Winkel D. (2012), Mixing over the steep side of the Cycladic Plateau in the Aegean Sea, *J. Mar. Syst.*, *89*(1), 30–47, doi:10.1016/j.jmarsys.2011.07.009.

Houpert, L., et al. (2016), Observations of open-ocean deep convection in the northwestern Mediterranean Sea: Seasonal and interannual variability of mixing and deep water masses for the 2007–2013 Period, *J. Geophys. Res. Oceans*, *121*, 8139–8171, doi:10.1002/2016JC011857.

Huussen, T. N., A. C. Naveira-Garabato, H. L. Bryden, and E. L. McDonagh (2012), Is the deep Indian Ocean MOC sustained by breaking internal waves?, *J. Geophys. Res.*, *117*, C08024, doi:10.1029/2012JC008236.

Lascaratos, A. (1993), Estimation of deep and intermediate water mass formation rates in the Mediterranean Sea, *Deep-Sea Res., Part II*, *40*(6), 1327-1332.

López-Jurado, J., C. Gonzalez-Pola, and P. Velez-Belchi (2005), Observation of an abrupt disruption of the long-term warming trend at the Balearic Sea, western Mediterranean Sea, in summer 2005, *Geophys. Res. Lett.*, *32*, L24606, doi:10.1029/2005GL024430.

McDougall, T. (1991), Parameterizing mixing in inverse models. Dynamics of ocean internal gravity waves, in *Proc. 'Aha Huliko'a Hawaiian Winter Workshop*, pp. 355–386, Univ. of Hawaii at Manoa, Honolulu, Hawaii.

McDougall, T., and Y. You (1991), Implications of the non-linear equation of state for upwelling in the ocean interior, *J. Geophys. Res.*, *95*, 13,263-13,276, doi:10.1029/JC095iC08p13263.

MEDOC Group (1970), Observation of formation of deep water in the Mediterranean Sea, 1969, *Nature*, *227*, 1037–1040.

Millot, C. (2009), Another description of the Mediterranean Sea outflow, *Prog. Oceanogr.*, *82*, 101–124.

Millot, C., and Taupier-Letage, I. (2005), *Circulation in the Mediterranean Sea. The Handbook of Environmental Chemistry*. 5(K), 29–66.

Mongelli, F., G. Zito, S. De Lorenzo, and C. Doglioni (2004), Geodynamic interpretation of the heat flow in the Tyrrhenian Sea, *Mem. Descr. Carta Geol. Ital.*, *44*, 71-82.

Morris, M. Y., M. M. Hall, L. C. St. Laurent, and N. G. Hogg (2001), Abyssal mixing in the Brazil Basin, *J. Phys. Oceanogr.*, *31*, 3331–3348.

Nash, J. D., E. Kunze, J. M. Toole, and R. W. Schmitt (2004), Internal tide reflection and turbulent mixing on the continental slope, *J. Phys. Oceanogr.*, *34*, 1117–1134, doi:10.1175/1520-0485.

Nielsen, J. N. (1912), *Hydrography of the Mediterranean and Adjacent Waters. Rep. Danish Oceanogr. Exped. 1908–1910*, pp. 72–191, Copenhagen.

Onken, R., A. R. Robinson, P. F. J. Lermusiaux, P. J. Haley Jr., and L. A. Anderson (2003), Data-driven simulations of synoptic circulation and transports in the Tunisia-Sardinia-Sicily region, *J. Geophys. Res.*, *108*(C9), 8123, doi:10.1029/2002JC001348.

Pasquale, V., M. Verdoya, and P. Chiozzi (1996a), Heat flux and timing of the drifting stage in the Ligurian–Provençal basin (NW-Mediterranean), *J. Geodyn.*, *21*(3), 205–222.
Pasquale, V., M. Verdoya, and P. Chiozzi (1996b), Some geophysical constraints to dynamic processes in the Southwestern Mediterranean, *Ann. Geofis.*, *39*(6), 1185–1200.
Pasquale, V., M. Verdoya, and P. Chiozzi (1999), Thermal state and deep earthquakes in the Southern Tyrrhenian, *Tectonophysics*, *306*, 435–448.
Pasquet, S., P. Bouruet-Aubertot, G. Reverdin, A. Turnherr, and L. St. Laurent (2016), Finescale parameterizations of energy dissipation in a region of strong internal tides and sheared flow, the Lucky-Strike segment of the Mid-Atlantic Ridge, *Deep Sea Res.*, *112*, 79–93, doi:10.1016/j.dsr.2015.12.016
Puig, P., et al. (2013), Thick bottom nepheloid layers in the western Mediterranean generated by deep dense shelf water cascading, *Prog. Oceanogr.*, *111*, 1-23, doi:10.1016/j.pocean.2012.10.003.
Polzin, K. L., J. M. Toole, J. R. Ledwell, and R. W. Schmitt (1997), Spatial variability of turbulent mixing in the abyssal ocean. *Science*, *276*, 93–96.
Rhein, M. (1995), Deep water formation in the western Mediterranean, *J. Geophys. Res.*, *100*(C4), 6943–6959, doi:10.1029/94JC03198.
Rohling, E. J., G. Marino, and K. M. Grant (2015), Mediterranean climate and oceanography, and the periodic development of anoxic events (sapropels), *Earth-Sci. Rev.*, *143*, 62–97.
Schroeder, K., G. P. Gasparini, M. Tangherlini, and M. Astraldi (2006), Deep and intermediate water in the Western Mediterranean under the influence of the Eastern Mediterranean Transient, *Geophys. Res. Lett.*, *33*, L21607, doi:10.1029/2006GL027121.
Schroeder, K., A. Ribotti, M. Borghini, R. Sorgente, A. Perilli, and G. P. Gasparini (2008), An extensive western Mediterranean deep water renewal between 2004 and 2006, *Geophys. Res. Lett.*, *35*, L18605, doi:10.1029/2008GL035146.
Schroeder, K., J. Chiggiato, H. L. Bryden, M. Borghini, and S. Ben Ismail (2016), Abrupt climate shift in the Western Mediterranean Sea, *Sci. Rep.*, *6*, 23009, doi:10.1038/srep23009.
Send, U., F. Schott, F. Gaillard, and Y. Desaubies (1995), Observation of a deep convection regime with acoustic tomography, *J. Geophys. Res.*, *100*(C4), 6927–6941, doi:10.1029/94JC03311.
Shih, L. H., J. R. Koseff, G. N. Ivey, and J. H. Ferziger (2005), Parameterization of turbulent fluxes and scales using homogeneous sheared stably stratified turbulence simulations, *J. Fluid Mech.*, *525*, 193–214, doi:10.1017/S0022112004002587.
Smith, R. O., H. L. Bryden, and K. Stansfield (2008), Observations of new western Mediterranean deep water formation using ARGO floats 2004–2006, *Ocean Sci.*, *4*, 133–149.
Smith, W. H. F., and D. T. Sandwell (1997), Global seafloor topography from satellite altimetry and ship depth soundings, *Science*, *277*, 1956–1962, doi:10.1126/science.277.5334.1956.
Somot, S., et al. (2016), Characterizing, modelling and understanding the climate variability of the deep water formation in the north-western Mediterranean sea, *Clim. Dyn.*, doi:10.1007/s00382-016-3295-0.
Sparnocchia, S., P. Picco, G. M. R. Manzella, A. Ribotti, S. Copello, and P. Brasey (1995), Intermediate water formation in the Ligurian Sea, *Oceanol. Acta*, *12*, 151–162.
Stommel H., H. Bryden, and P. Mangelsdorf (1973), Does some of the Mediterranean outflow come from great depth?, *Pure Appl. Geophys.*, *105*, 879-889.
Tchernia, P. (1956), Contribution à l'étude hydrologique de la Méditerranée Occidentale, Bull. Inform. Com. Ocean. Etudes Côtes, 8, 9.I.G.
Testor, P., and J.-C. Gascard (2003), Large-scale spreading of deep waters in the Western Mediterranean Sea by submesoscale coherent eddies, *J. Phys. Oceanogr.*, *33*, 75-87.
Testor, P., and J.-C. C. Gascard (2006), Post-convection spreading phase in the Northwestern Mediterranean Sea, *Deep Sea Res., Part I*, *53*(5), 869-893, doi:10.1016/j.dsr.2006.02.004.
Tziperman, E., and K. Speer (1994), A study of water mass transformation in the Mediterranean Sea: Analysis of climatological data and a simple three-box model, *Dyn. Atmos. Oceans*, *21*, 53-82.
Ulses, C., C. Estournel, P. Puig, X. Durrieu de Madron, and P. Marsaleix (2008), Dense water cascading in the northwestern Mediterranean during the cold winter 2005. Quantification of the export through the Gulf of Lion and the Catalan margin, *Geophys. Res. Lett.*, *35*, L07610, doi:10.1029/2008GL033257.
Waldman R., et al. (2016), Estimating dense water volume and its evolution for the year 2012–2013 in the Northwestern Mediterranean Sea: An observing system simulation experiment approach. *J. Geophys. Res. Oceans*, *121*, 6696–6716, doi:10.1002/2016JC011694.
Whalen, C. B., L. D. Talley, and J. A. MacKinnon (2012), Spatial and temporal variability of global ocean mixing inferred from Argo profiles, *Geophys. Res. Lett.*, *39*, L18612, doi:10.1029/2012GL053196.
Wüst, G. (1961), On the vertical circulation of the Mediterranean Sea, *J. Geophys. Res.*, *66*, 3261-3271, doi:10.1029/JZ066i010p03261.